HAL
open science

Vlasov laser-plasma interaction simulations with a moving grid

Nicolas Crouseilles, Alain Ghizzo, Stéphanie Salmon

To cite this version:

Nicolas Crouseilles, Alain Ghizzo, Stéphanie Salmon. Vlasov laser-plasma interaction simulations with a moving grid. [Research Report] RR-6109, INRIA. 2007. inria-00127747v2

HAL Id: inria-00127747

https://inria.hal.science/inria-00127747v2

Submitted on 30 Jan 2007

HAL is a multi-disciplinary open access archive for the deposit and dissemination of scientific research documents, whether they are published or not. The documents may come from teaching and research institutions in France or abroad, or from public or private research centers.

L'archive ouverte pluridisciplinaire **HAL**, est destinée au dépôt et à la diffusion de documents scientifiques de niveau recherche, publiés ou non, émanant des établissements d'enseignement et de recherche français ou étrangers, des laboratoires publics ou privés.

INSTITUT NATIONAL DE RECHERCHE EN INFORMATIQUE ET EN AUTOMATIQUE

Vlasov laser-plasma interaction simulations in the relativistic regime with a moving grid

Nicolas Crouseilles — Alain Ghizzo — Stéphanie Salmon

N° 6109

Janvier 2007

Thème NUM

Rapport de recherche

ISSN 0249-6399

Vlasov laser-plasma interaction simulations in the relativistic regime with a moving grid

Nicolas Crouseilles*, Alain Ghizzo †, Stéphanie Salmon ‡

Thème NUM — Systèmes numériques
Projet CALVI

Rapport de recherche n° 6109 — Janvier 2007 — 22 pages

Abstract: The present work focuses on the numerical resolution of a reduced 1D Vlasov-Maxwell system introduced recently in the physical literature for studying laser-plasma interaction. This system can be seen as a standard Vlasov equation in which the force term is split into two terms: the classical electrostatic field obtained from the Poisson's equation and a magnetic term evolving through Maxwell's type equations. A semi-Lagrangian code is used to study the interaction of ultrashort electromagnetic pulse with plasma; however during the major part of the simulation, many of the grid points are wasted. We then introduce a dynamic mesh which allows us to consider the part of the phase space where the distribution function is not zero.

Key-words: Vlasov equation, semi-Lagrangian method, relativistic regime, moving grid

* INRIA-Lorraine, Projet CALVI
† LPMIA-Nancy
‡ IRMA-Strasbourg et INRIA-Lorraine, Projet CALVI

Unité de recherche INRIA Lorraine
LORIA, Technopôle de Nancy-Brabois, Campus scientifique,

Simulations numériques d'interaction laser-plasma dans un régime relativiste grâce à un maillage mobile

Résumé : Ce travail concerne la résolution numérique d'un modèle unidimensionnel Vlasov-Maxwell récemment obtenu dans la littérature physique pour étudier l'interaction laser-plasma. Ce modèle peut être vu comme une équation de type Vlasov où le terme de force contient deux termes : d'une part le champ électrique résolvant l'équation de Poisson et d'autre part un terme de champ magnétique évoluant à travers les équations de Maxwell. Un code semi-Lagrangien est alors utilisé pour simuler l'interaction d'un tir électromagnétique ultra-court avec un plasma ; cependant, durant la majeure partie de la simulation, la plupart des points de la grille de l'espace des phases est gaspillée. Dans ce travail, on introduit une grille dynamique de l'espace des phases qui contient les points où la fonction de distribution est non nulle.

Mots-clés : équation de Vlasov, méthode semi-Lagrangienne, physique relativiste, maillage mobile

1 Introduction

The Vlasov equation describes the evolution of a system of charged particles under the effects of self-consistent or applied electromagnetic fields. The unknown f is a distribution function of particles in the phase space which depends on the time $t \geq 0$, the physical space $x \in \mathbb{R}^d$ and the momentum $p \in \mathbb{R}^d$, where d is the dimension $d = 1, 2, 3$. This kind of model can be used for the study of beam propagation, relativistic, collisionless or gyrokinetic plasmas.

The numerical resolution of Vlasov type equations, the solution of which depends at least on 6 variables plus time, is performed most of the time using particle methods (Particle In Cell methods) where the plasma is approached by a finite number of macro-particles. The trajectories of these particles are computed using the characteristic curves given by the Vlasov equation, whereas the electromagnetic fields are computed on a fixed grid [2]. But thanks to the increase of computing power in the last decades, simulations of plasmas or particle beams based on direct solution of the Vlasov equation on a multi-dimensional grid are becoming attractive as an alternative to the particle methods. In particular, when one wants to study low-density regions, Vlasov methods seem to be more precise since they are noiseless and all parts of phase space are equally well resolved.

Eulerian methods have proven their efficiency on uniform meshes in two-dimensional phase space, but when the dimensionality increases, the number of points on a uniform grid becomes very important which makes numerical simulations challenging. For inhomogeneous systems however, many of the grid points (where no particles are present) are wasted and this makes the Vlasov simulations particularly inefficient. This is especially the case for beam simulations where the beam moves rapidly through the phase space (due to varying alternating-gradient focusing forces, for example), or in many relativistic contexts modeling laser-plasma interaction. In such situations, a smaller grid can be introduced so that it contains the whole information at a given time. This concept of moving grid, introduced in [13], does not consider the points with vanishing values of the distribution function. The distribution function is computed on this moving grid whereas the electromagnetic fields are computed on the whole classical grid.

This work is devoted to the implementation of the moving grid strategy to efficiently solve a one-dimensional Vlasov-Maxwell model. To that purpose, a semi-Lagrangian method is used (see [5, 14]). which consists in updating the values of the distribution function at the nodes of the grid by following the characteristics ending at these nodes backward, and interpolating the value at the bottom of the characteristics from the known values at the previous step (see [5, 14]). The one-dimensional Vlasov-Maxwell model considers a population of relativistic electrons and describes laser-plasma interaction. This kinetic model has been introduced recently in the physical literature (see [11, 7]) and can be written (considering the electronic distribution function $f = f(t, x, p)$) as follows

$$\frac{\partial f}{\partial t} + \frac{p}{m\gamma}\frac{\partial f}{\partial x} + e\left(E_x - \frac{mc^2}{2\gamma}\frac{\partial a^2}{\partial x}\right)\frac{\partial f}{\partial p} = 0, \tag{1.1}$$

where $\gamma = \sqrt{1 + (p^2/m^2c^2) + a^2}$ is the Lorentz factor and $a(t,x) = eA(t,x)/mc$ is the normalized amplitude of the potential vector $A = (0, A_y, A_z)$. We denote by m the electronic mass, c the light velocity and e the electronic charge. The Vlasov equations (1.1) has to be considered with its coupling with the Maxwell's equations. This system can be seen as a standard Vlasov equation in which the force term is split into two terms: the usual electrostatic field obtained from Poisson's equation and the magnetic term evolving through Maxwell's equations. The main assumptions to obtain the one-dimensional model are the following: all variables depend on only one space variable, denoted x, and the electrons are monokinetic in the direction transversal to x. The justification of these assumptions comes from the fact that all the interesting phenomena are much more rapid along the direction of propagation of the laser wave than in the transversal directions. Moreover, since ion motion can be neglected during very short lasers pulses ($< 1\ ps.$), we only need to consider electron motion. All the details for obtaining these equations have been extensively described in [11, 7].

Numerical simulations are performed using the moving grid method, to simulate the one-dimensional model (1.1) in the context related to the study of parametric instability induced by an intense pump electromagnetic wave. To describe in detail the wave-particle interaction, we use a semi-Lagrangian code considering periodic boundary conditions in the case of a circularly polarized electromagnetic wave. On the one side, we make some comparisons with the analytical value of the growth rate of the instability in the relativistic regime. On the other side, comparisons are also performed with a classical semi-Lagrangian algorithm (see [9, 6, 7]). This test can be viewed as a preliminary work before the application to the simulations of more realistic causal case in which propagation of a relativistically strong laser pulse in a moderately overdense plasma is studied. As a result of recent progress in optical processing, this kind of test is of particular interest in the inertial confinement fusion for example.

For the sake of completeness, we also mention others methodologies recently implemented to avoid the increasing of points using uniform grid. For example, adaptive methods decrease the computational cost by refining some grid regions where thin structures are expected to develop and derefining zones where the distribution function is smooth. Such adaptive methods use moving distribution function grids well suited to manage data locality. For more details, we refer the reader to [1, 3, 8].

The paper is organized as follows: first we present more precisely the one-dimensional Vlasov-Maxwell model; the semi-Lagrangian method is introduced in section 3. Then we describe the moving grid methodology applied to the 1D Vlasov-Maxwell model and finally present its application to numerical simulations of laser-plasma interaction.

2 The Vlasov equation

In this section, we introduce the Vlasov-Maxwell model, whose derivation can be found in details in [11, 7]. Considering the electronic distribution function $f = f(t, x, p)$ which depends on the physical space $x \in [0, L_x]$ and the momentum $p \in \mathbb{R}$, the one-dimensional Vlasov model reads

$$\frac{\partial f}{\partial t} + \frac{p}{m\gamma}\frac{\partial f}{\partial x} + e\left(E_x - \frac{mc^2}{2\gamma}\frac{\partial a^2}{\partial x}\right)\frac{\partial f}{\partial p} = 0, \tag{2.2}$$

where $\gamma = \sqrt{1 + (p^2/m^2c^2) + a^2}$ is the Lorentz factor and $a(t, x) = eA(t, x)/mc$ is the normalized amplitude of the potential vector $A = (0, A_y, A_z)$. The physical constants are detailed in the introduction. The Vlasov equation has to be considered with its coupling with the Maxwell's equations

$$\frac{\partial E_y(t,x)}{\partial t} = -c^2\frac{\partial B_z(t,x)}{\partial x} + \omega_p^2 A_y(t,x)\rho_\gamma(t,x), \quad \frac{\partial E_z(t,x)}{\partial t} = c^2\frac{\partial B_y(t,x)}{\partial x} + \omega_p^2 A_z(t,x)\rho_\gamma(t,x) \tag{2.3}$$

$$\frac{\partial B_y(t,x)}{\partial t} = \frac{\partial E_z(t,x)}{\partial x}, \qquad \frac{\partial B_z(t,x)}{\partial t} = -\frac{\partial E_y(t,x)}{\partial x}, \tag{2.4}$$

where ω_p is the usual plasma frequency and

$$\rho_\gamma(t,x) = \int_{\mathbb{R}} \frac{f(t,x,p)}{m\gamma}dp.$$

The components of the potential vector are then computing using

$$\frac{\partial A_y(t,x)}{\partial t} = -E_y(t,x), \qquad \frac{\partial A_z(t,x)}{\partial t} = -E_z(t,x). \tag{2.5}$$

The longitudinal component of the electric field is obtained by solving Poisson's equation (where n_i is the constant ionic density)

$$\frac{\partial E_x(t,x)}{\partial x} = \frac{e}{\epsilon_0}\left(\int_{\mathbb{R}} f(t,x,p)dp - n_i\right), \tag{2.6}$$

or equivalently the Ampère equation

$$\frac{\partial E_x(t,x)}{\partial t} = -J(t,x), \tag{2.7}$$

where the current $J(t, x)$ is given by

$$J(t,x) = \int_{\mathbb{R}} \frac{pf(t,x,p)}{m\gamma}dp.$$

Let us remark that (2.6) and (2.7) are relative to the same variable E_x and are redondant under regularity conditions. As usual, the satisfaction of equation (2.6) at $t = 0$ implies

(at the continuous level) its satisfaction at any time thanks to (2.7) and to the continuous equation $\partial_t \rho + \partial_x J = 0$, with $\rho(t,x) = \int f(t,x,p)dp$.

In this paper, we focus on the one-dimensional Vlasov equation (2.2) well suited to describe laser-plasma interaction. This model has been both theoritically and numerically studied. Indeed, in [12], the authors investigate the existence and the uniqueness of solutions in a slightly simplified framework. Moreover, numerical study using the semi-Lagrangian method can be found in [9, 6, 7]; in particular in [9], the authors proved that the time splitting leads to numerical instabilities that are not physical.

3 The semi-Lagrangian method for the Vlasov equation

3.1 The semi-Lagrangian method

The semi-Lagrangian method consists in computing approximation of the solution of the Vlasov equation (2.2) on a phase space grid by using the property of the equation that the distribution function f is conserved along characteristics. More precisely, for any times s and t, we have

$$f(t,x,v) = f(s, X(s;t,x,v), V(s;t,x,v)),$$

where $(X(s;t,x,v), V(s;t,x,v))$ are the characteristics of the Vlasov equation which are solution of the system of ordinary differential equations

$$\left\{ \begin{array}{rcl} \dfrac{dX}{ds} & = & V, \\ \\ \dfrac{dP}{ds} & = & \mathcal{F}(s, X(s), P(s)), \end{array} \right. \tag{3.8}$$

where $\mathcal{F}$ denotes the force term in the Vlasov equation (2.2). The system (3.8) is supplemented with the initial conditions

$$X(t) = x, \quad V(t) = v.$$

From this property, f^n being known one can introduce a numerical method for computing the distribution function f^{n+1} at the grid points (x_i, v_j) consisting in two steps

1. Find the starting point of the characteristic curves ending at (x_i, v_j): $X(t^n; x_i, v_j, t^{n+1})$ and $V(t^n; x_i, v_j, t^{n+1})$.

2. Compute $f(t^n, X^n, V^n)$ by interpolation, f being known only at mesh points at time t^n.

In order to deal with the first step, a time discretization of (3.8) has to be performed using a high enough order (the second order seems to be sufficiently accurate). To treat the second step, one has to choose an interpolation operator. Even if the semi-Lagrangian method does not require any specific interpolation scheme, numerical experiences dictate the

use of high order methods so that diffusion is limited. Cubic splines or Lagrange polynomials for example present some good properties and seem to be a good compromise between a small diffusivity and a low computational cost.

3.2 Why does the splitting fail ?

The time splitting procedure, introduced in [4] allows a straightforward resolution of the characteristic curves, but the algorithm is valid provided that the equation fulfils some conditions. Unfortunately, the one-dimensional relativistic model requires the resolution of a two-dimensional interpolation since the time splitting can not be applied in this model (see [9]). Indeed, starting with the conservative form of the Vlasov equation (2.2) thanks to the following property of the advection field

$$\nabla_X \cdot (U(t,X)) = 0, \quad \text{with} \quad U(t,X) = (U_1(t,X), U_2(t,X)) = \left(\frac{p}{m\gamma}, e\left(E - \frac{mc^2}{2\gamma}\frac{\partial a^2}{\partial x}\right)\right),$$

with $X = (x,p)$. It is well known (see [4]) that solving separately

$$\frac{\partial f}{\partial t} + \frac{\partial}{\partial x}\left(\frac{p}{m\gamma} f\right) = 0, \tag{3.9}$$

and

$$\frac{\partial f}{\partial t} + \frac{\partial}{\partial p}\left[e\left(E - \frac{mc^2}{2\gamma}\frac{\partial a^2}{\partial x}\right) f\right] = 0, \tag{3.10}$$

keeps the second-order accuracy in time for the whole (2.2) equation by alternating the solves. Now, we point out that the semi-Lagrangian method does not solve Vlasov's equations in the conservative form but in the advective form. Therefore, if and only if both conditions hold

$$\frac{\partial U_1}{\partial x} = 0, \quad \frac{\partial U_2}{\partial p} = 0,$$

equations (3.9) and (3.10) can be put in the advective form

$$\frac{\partial f}{\partial t} + U_1 \frac{\partial f}{\partial x} = 0, \quad \frac{\partial f}{\partial t} + U_2 \frac{\partial f}{\partial p} = 0,$$

allowing to keep the second-order accuracy. Unfortunately, the presence of the Lorentz factor γ couples the variables x and p and prevents the fields U_1 and U_2 to be divergence free, since

$$\frac{\partial U_1}{\partial x} = \frac{\partial}{\partial x}\left(\frac{p}{m\gamma}\right) = -\frac{p}{2m\gamma^3}\frac{\partial a}{\partial x} \neq 0,$$

and

$$\frac{\partial U_2}{\partial p} = \frac{\partial}{\partial p}\left(e\left(E_x - \frac{mc^2}{2\gamma}\frac{\partial a^2}{\partial x}\right)\right) = -\frac{\partial U_1}{\partial x} \neq 0.$$

On the contrary, in the nonrelativistic case $\gamma = 1$, the divergence conditions hold for U_1 and U_2. The numerical proof of the fact that the time splitting is inadequate when high intensity laser are considered has been done in [9]. In particular, using a time splitting introduces a cumulative error at each time step resulting in poor density conservation.

3.3 Algorithms for the 1D Vlasov-Maxwell system

As we saw above, the grid transformations mixes space and velocity components, and an efficient method for solving the characteristics without splitting has to be used to remain accurate in time. A possible option would be to use the time-steps method introduced in [14]; this leap-frog algorithm that is detailed in the sequel has the advantage to be second order in time, but it has the drawback of decoupling even and odd time steps. Moreover, for each time step, two interpolation procedure are required, which is quite costly. Then, we use a second order predictor-corrector numerical scheme using the Ampère equation (2.7) to advance the longitudinal electric field, which allows to advance the perpendicular electromagnetic fields. At the end of each time step, the predicted longitudinal electric field is replaced by the real solution of the Poisson equation at time t^{n+1}.

In this subsection, we present two different algorithms which have been implemented to perform the numerical simulations. Notice that, for the sake of clarity, all physical constants have been omitted.

Leap-frog algorithm

Knowing the final position (X^{n+1}, V^{n+1}) at time step t^{n+1}, as well as $f^n, f^{n+1/2}, f^{n-1}, E_y^{n-1/4}$, $E_z^{n-1/4}, B_y^n, B_z^n, A_y^n, A_z^n$, we can compute the initial position (X^n, V^n) using the following algorithm.

First step

1.1 Advance the electric field using (2.3) on a half time step from $E_y^{n-1/4}$ (resp. $E_z^{n-1/4}$) to get $E_y^{n+1/4}$ (resp. $E_z^{n+1/4}$) using $\rho_\gamma^n, A_y^n, B_y^n$ (resp. $\rho_\gamma^n, A_z^n, B_z^n$).

1.2 Advance the magnetic fields using (2.4) on a half time step B_y^n (resp. B_z^n) to get $B_y^{n+1/2}$ (resp. $B_z^{n+1/2}$) using $E_y^{n+1/4}$ (resp. $E_z^{n+1/4}$).

1.3 Advance the potential vector using (2.5) on a half time step A_y^n (resp. A_z^n) to get $A_y^{n+1/2}$ (resp. $A_z^{n+1/2}$) using $E_y^{n+1/4}$ (resp. $E_z^{n+1/4}$).

1.4 Solve the Poisson equation at time $t^{n+1/2}$ using $f^{n+1/2}$ to get $E_x^{n+1/2}$.

1.5 Compute the force term at time $t^{n+1/2}$, push backwards the characteristic curves following step 6. of the previous algorithm, and interpolate the distribution function to get f^{n+1} using f^n.

Second step

2.1 Advance the electric field using (2.3) on a half time step from $E_y^{n+1/4}$ (resp. $E_z^{n+1/4}$) to get $E_y^{n+3/4}$ (resp. $E_z^{n+3/4}$) using $\rho_\gamma^{n+1/2}, A_y^{n+1/2}, B_y^{n+1/2}$ (resp. $\rho_\gamma^{n+1/2}, A_z^{n+1/2}, B_z^{n+1/2}$).

2.2 Advance the magnetic fields using (2.4) on a half time step $B_y^{n+1/2}$ (resp. $B_z^{n+1/2}$) to get B_y^{n+1} (resp. B_z^{n+1}) using $E_y^{n+3/4}$ (resp. $E_z^{n+3/4}$).
2.3 Advance the potential vector using (2.5) on a half time step $A_y^{n+1/2}$ (resp. $A_z^{n+1/2}$) to get A_y^{n+1} (resp. A_z^{n+1}) using $E_y^{n+3/4}$ (resp. $E_z^{n+3/4}$).
2.4 Solve the Poisson equation at time t^{n+1} using f^{n+1} to get E_x^{n+1}.
2.5 Compute the force term at time t^{n+1}, push backwards the characteristic curves following step 6. of the previous algorithm and interpolate the distribution function to get $f^{n+3/2}$ using $f^{n+1/2}$.
Averaging step: Average the two obtained distribution functions to get f^{n+1}

$$f^{n+1} = \frac{1}{2}(f^{n+1/2} + f^{n+3/2}).$$

Ampère algorithm

Knowing the final position (X^{n+1}, V^{n+1}) at time step t^{n+1}, as well as $f^n, E_x^{n-1/2}, E_y^{n-1/2}$, $E_z^{n-1/2}, B_y^n, B_z^n, A_y^n, A_z^n$, we can compute the initial position (X^n, V^n) using the following algorithm.
1. Advance the electric field using (2.3) on a time step from $E_y^{n-1/2}$ (resp. $E_z^{n-1/2}$) to get $E_y^{n+1/2}$ (resp. $E_z^{n+1/2}$) using $\rho_\gamma^n, B_z^n, A_y^n$ (resp. $\rho_\gamma^n, B_y^n, A_z^n$). Hence the Yee scheme reads

$$E_{y,i}^{n+1/2} = E_{y,i}^{n-1/2} - \frac{\Delta t}{\Delta x}(B_{z,i+1/2}^n - B_{z,i-1/2}^n) + \Delta t A_{y,i}^n \rho_{\gamma,i}^n,$$

for E_y

$$E_{z,i}^{n+1/2} = E_{z,i}^{n-1/2} - \frac{\Delta t}{\Delta x}(B_{y,i+1/2}^n - B_{y,i-1/2}^n) + \Delta t A_{z,i}^n \rho_{\gamma,i}^n,$$

for E_z.
2. Advance the magnetic field using (2.4) on a time step from B_y^n (resp. B_z^n) to get B_y^{n+1} (resp. B_z^{n+1}) using $E_y^{n+1/2}, E_z^{n+1/2}$. Then, we have

$$B_{y,i-1/2}^{n+1} = B_{y,i-1/2}^n - \frac{\Delta t}{\Delta x}(E_{y,i}^{n+1/2} - E_{y,i-1}^{n+1/2}),$$

for B_y and

$$B_{z,i-1/2}^{n+1} = B_{z,i-1/2}^n - \frac{\Delta t}{\Delta x}(E_{z,i}^{n+1/2} - E_{z,i-1}^{n+1/2}),$$

for B_z.
3. Advance the potential vector using (2.5) on a time step from A_y^n (resp. A_z^n) to get A_y^{n+1} (resp. A_z^{n+1}) using $E_y^{n+1/2}, E_z^{n+1/2}$. We obtain

$$A_{y,i}^{n+1} = A_{y,i}^n - \Delta t E_{y,i}^{n+1/2},$$

for A_y and

$$A_{z,i}^{n+1} = A_{z,i}^{n} - \Delta t E_{z,i}^{n+1/2},$$

for A_z.
4. Advance the longitudinal electric field using (2.7) on a time step from $E_x^{n+1/2}$ to get $E_x^{n-1/2}$ using J_x^n

$$E_{x,i}^{n+1/2} = E_{x,i}^{n-1/2} - \Delta t J_{x,i}^{n}.$$

5. Compute the force field at time $t^{n+1/2}$

$$\mathcal{F}_i^{n+1/2} = \left(E_x^{n+1/2} - \frac{1}{\gamma_i^{n+1/2}} (A_{y,i}^{n+1/2} B_{z,i}^{n+1/2} - A_{z,i}^{n+1/2} B_{y,i}^{n+1/2}) \right),$$

where the magnetic fields B and A are estimated at time $t^{n+1/2}$ by averaging times t^n and t^{n+1}, B_y and B_z are evaluated at x_i by averaging their values at $x_{i+1/2}$ and $x_{i-1/2}$; finally $\gamma_i^{n+1/2}$ is the Lorentz factor at time $t^{n+1/2}$

$$\gamma_i^{n+1/2} = \sqrt{1 + p^2 + (A_{y,i}^{n+1/2})^2 + (A_{z,i}^{n+1/2})^2}.$$

6. Integrating the nonlinear ODE $\partial_t z(t) = F(t, z(t))$ with $z(t) = (x(t), p(t))$ and $F(t, z(t)) = (p(t)/\gamma, \mathcal{F}(t, x(t), p(t)))$ on the interval $[t^n, t^{n+1}]$ using a middle point quadrature rule, we are leading to solve the following fixed-point problem in (δ_x, δ_p)

$$\delta_z = \Delta t F(t^{n+1/2}, z(t^{n+1}) - \delta_z/2),$$

denoting by δ_z the two-dimensional displacement between $z(t^{n+1})$ and the bottom of the charateristics $z(t^n)$.
7. Interpolate the distribution function at time f^n to get f^{n+1} using the force term $\mathcal{F}^{n+1/2}$.
8. Correction of the longitudinal electric field E_x using the Poisson equation at time t^{n+1} and t^n

$$E_x^{n+1/2} = \frac{1}{2}(E_x^{n+1} + E_x^{n}).$$

Remark 3.1 *The force term computed at step* 5 *of the first algorithm is totally consistent with the force term in equation (2.2). Indeed, by differentiating equations (2.5) with respect to x, and by combining equations (2.4), we obtain*

$$\frac{\partial^2 A_y(t,x)}{\partial t \partial x} = -\frac{\partial B_z}{\partial t}, \quad \frac{\partial^2 A_z(t,x)}{\partial t \partial x} = \frac{\partial B_y}{\partial t}.$$

Then, the second part of the force term can be re-written as follows

$$\begin{aligned} a(t,x)\frac{\partial a(t,x)}{\partial x} &= A_y(t,x)\frac{\partial A_y(t,x)}{\partial x} + A_z(t,x)\frac{\partial A_z(t,x)}{\partial x} \\ &= -A_y(t,x)B_z(t,x) + A_z(t,x)B_y(t,x). \end{aligned}$$

This last expression is used in the numerical scheme to approach the magnetic component of the force term.

For both algorithms, a second order in time is reached. For the interpolation step, a standard cubic splines approximation is done (see [14]).

4 The moving grid algorithm

The reduced Vlasov-Maxwell system has been studied from a numerical point of view in [9, 6, 7]. One of the conclusion of these works lead to the fact that Eulerian approach seems to be well suited to this kind of situations since they are noiseless and a fine mesh allows to capture thin structures developed by the distribution function.

In the fully relativistic regime considered here, perturbation theory can not take into account nonlinearities of the primary wave since the studied instability has a very strong rate. Hence, a global equilibrium is imposed at the beginning which remains stable for a long time and after, the instability occurs and grows rapidly (where thin structures are located). In such a situation, the Maxwellian equilibrium does not need a very precise description, but in prevision of the beginning of the instability, a very fine grid and a large domain are required during all the simulation, which make the simulation very costly from a CPU time point of view. Hence the concept of the moving grid introduced in [13] where the grid is mapped at each time step seems to be adapted; this time dependant moving grid is chosen so that it contains the major information of the whole distribution function at a given time.

In this work, we try to construct a simple dynamic grid of the phase space that is adapted to the form of the distribution function at each time step. Within the framework of this paper, the space direction is fixed to $[0, L_x]$, whereas a criterion on the distribution function allows us to modify the impulsion domain with time; so, the phase space domain $[0, L_x] \times [p_{min}(t), p_{max}(t)]$, $(t \geq 0)$ will be considered during the simulation. Like in [6], we choose initially a symmetric impulsion domain ($p_{min}(t = 0) = -p_{max}(t = 0)$) with $p_{max} = 2.5$. We also consider $N_p \approx 700$ points in this direction. The criterion is the following: let us introduce the p-projection of the distribution function

$$F(t = 0, p) = \int_0^{L_x} f(t = 0, x, p)\, \mathrm{d}x, \quad p \in [p_{min}(t = 0), p_{max}(t = 0)],$$

where $[0, L_x]$ is the space domain. Let us also define a threshold ε. Then the criterion is

$$\text{While } F(t = 0, p_{max}(t = 0)) < \varepsilon,$$

$$p_{max}(t = 0) = p_{max}(t = 0) - 2\Delta p.$$

Then, we preserve the initial resolution (*i.e.* the initial Δp), but the maximum value of the impulsion is decreased such that we only keep values of $F(t = 0, p)$ that remain significative. For example, some numerical experiments show that the previous algorithm together with the choice of $\varepsilon = 10^{-10}$ leads to $p_{max}(t = 0) = 0.5$ (instead of $p_{max}(t = 0) = 2.5$) and

then considers *five times less points* than initially. The initial distribution function is then sampled with the same precision (the same Δp is used), on a smaller domain; the new total mass is very similar from the one computed using the large domain $[-2.5, 2.5]$. The macroscopic quantities are then computed on the small domain; for example, the density is given by

$$\rho(t=0,x) = \int_{p_{min}(t=0)}^{p_{max}(t=0)} f(t=0,x,p)dp.$$

Obviously, others criteria can also be envisaged.

Hence, the simulation starts with a new momentum domain $[-p_{min}(t=0), p_{max}(t=0)]$ that is adapted to the distribution function at time $t=0$. The same kind of procedure is performed at the beginning of each time step $t^n = n\Delta t$ to predict the impulsion domain that is adapted to the distribution function at the next time step. We consider the projection onto the impulsion domain at time t^n

$$F(t=t^n,p) = \int_0^{L_x} f(t=t^n,x,p)\,\mathrm{d}x.$$

The criterion at time $t=t^n$ then writes

$$\text{If } F(t=t^n, p_{max}(t=t^n)) > \varepsilon,$$

$$\text{then } p_{max}(t=t^{n+1}) = p_{max}(t=t^n) + 2\Delta p,$$

$$f(t=t^n, x, \pm p_{max}(t=t^{n+1})) = 0, \quad f(t=t^n, x, \pm p_{max}(t=t^{n+1}) \mp \Delta p) = 0,$$

$$\text{else } p_{max}(t=t^{n+1}) = p_{max}(t=t^n).$$

A new domain is then predicted at the beginning of the time step, which will be able to take into account new structures developing from a time step to the following by the distribution function. The previous algorithms (Ampère and leap frog algorithms) are then used to solve the Vlasov equation considering the predicted impulsion domain.

Hence, when nothing occured, the impulsion domain remains unchanged (case 'else'), but when the test is fulfilled (case 'if'), the domain is extended with two cells on each side to preserve the symmetry of the problem. With this choice, the impulsion step Δp remains the same during all the simulation. Moreover the distribution function is always sampled on the same subjacent grid, so that there is no costly interpolation step to map the distribution function from the grid at time t^n to the grid at time t^{n+1}, or to compute the macroscopic quantities on a logical grid as in [13].

Moreover, we impose that the distribution function is equal to zero at the new cells $\pm p_{max}(t^{n+1})$, $p_{max}(t^{n+1}) - \Delta p$ and $-p_{max}(t^{n+1}) + \Delta p$, at the beginning of the time step. These values are then updated during the resolution of the Vlasov equation since all the algorithm takes into account the new number of cells in the impulsion direction.

As we shall see in the next section with numerical results, the size of the impulsion domain remains constant equal to $[-0.5, 0.5]$ (instead of $[-2.5, 2.5]$ in the usual case, involving five

times more points) during the major part of the simulation; then when the instability is developing, the domain is increasing to follow the created structures, to reach at the end of the simulation a value which is very near the constant value proposed by [6] (approximatively equal to 2.5). In some sense, this observation validates our choice of criterion.

5 Numerical results

In this section, some numerical results obtained with the methodology we exposed above are presented. Three different configurations are compared: the Leap-frog algorithm, the Ampère algorithm and the Ampère algorithm coupled with the dynamic moving grid. The relativistic test we study here has been introduced in [1, 6, 9].

5.1 Physical and numerical parameters

We briefly recall the physical and numerical parameters used to perform this test. We start with an initial homogeneous Maxwellian distribution function with a temperature $T = 3\,keV$, without perturbation term:

$$f_0(x,p) = \frac{n}{\sqrt{2\pi}T}\exp(-p^2/(2T^2)),$$

with n the electronic density and take the following initial conditions to describe the circularly polarized electromagnetic field

$$E_y^0(x) = E_0\cos(k_0\,x) \qquad E_z^0(x) = E_0\sin(k_0\,x)$$

$$B_y^0(x) = -\frac{k_0^\star E_0}{\omega_0}\sin(k_0\,x) \quad B_z^0(x) = \frac{k_0^\star E_0}{\omega_0}\cos(k_0\,x)$$

$$P_y^0(x) = -\frac{E_0}{\omega_0}\sin(k_0\,x) \qquad P_z^0(x) = \frac{E_0}{\omega_0}\cos(k_0\,x)$$

where $k_0^\star = k_0\mathrm{sinc}\,(\frac{k_0\Delta x}{2})$, with sinc $x = (\sin x)/x$. We consider a pump wave of frequency ω_0 and wavenumber k_0 such that the relativistic dispersion relation $\omega_0^2 = \omega_p^2/\gamma_0 + k_0^2c^2$ is satisfied, with $\gamma_0 = 1 + a_{osc}^2$, with a_{osc} the quiver momentum. By choosing $k_0c/m = 1/\sqrt{2}$ and $a_{osc} = \sqrt{3}$ (which corresponds to an irradiation of $I = 8\times10^8\,Wcm^{-2}$, we obtain $\omega_0/\omega_p = 1$ (*i.e.* a ratio of the plasma density to the critical density of $n/n_c = 1$). The choice of k_0 determines the size of the periodic space domain which is taken equal to $[0, 2\pi/\sqrt{2}]$. These parameters corresponds to the most unstable mode, the growth rate of which is $\gamma = 0.409$ (see [9, 10]).

The numerical parameters are chosen as follows: the impulsion domain is equal to $[-p_{max}, p_{max}]$, with $p_{max} = 2.5$ for uniform cases and $p_{max}^0 = 0.5$ for the dynamic moving grid case. The number of grid points is equal to 512 in the physical space whereas 768 points are considered in the impulsion domain for uniform cases. On the other side, 155 points are

considered in the dynamic moving grid case, in order to respect the uniform resolution (the impulsion step is then the same in the three cases). Finally, the time step is $dt = 0.01$ and the simulation runs during 10000 time steps.

5.2 Results

In this section, we present a numerical comparison of the three algorithms for the relativistic parametric instability with the initial condition presented above. First, notice in Fig. 1, Fig. 2, Fig. 3 that all the physical values, as mass, energy and entropy, present the same evolution in time. In particular, this means that the instability occurs at the same moment, with the Ampère algorithm on the one hand, and with the moving grid on the other hand.

On Fig. 4, we have plotted the time evolution of the most unstable plasma mode (mode 2) on a logarithmic scale: the curves corresponding to the three algorithms indicate a growth rate of $\gamma_{num} \approx 0.4$ which is in very good agreement with the expected value predicted by the linear theory (it i.e. $\gamma = 0.409$).

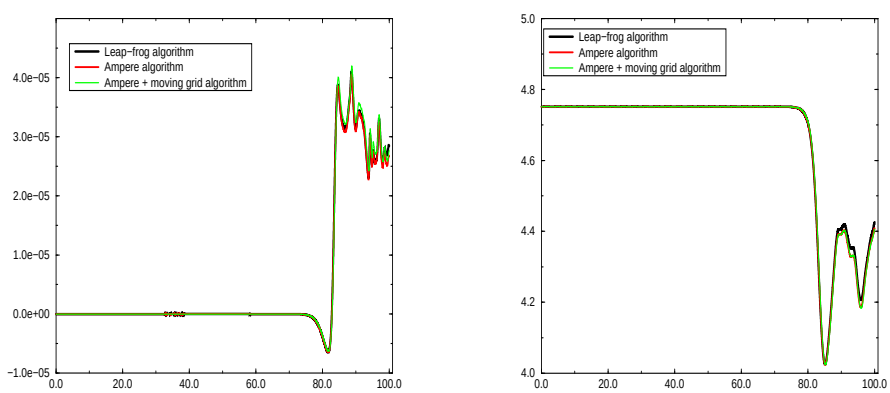

Figure 1: *Time evolution of the mass and the total energy.*

We present in Fig. 5 and Fig. 6 the time evolution of the distribution function f in the phase space obtained with the uniform algorithm. Between times $t = 0\,\omega_p^{-1}$ and $t = 70\,\omega_p^{-1}$, the function is a Maxwellian and occupies a very thin part of the phase space domain. Then, the instability occurs between $t = 70\,\omega_p^{-1}$ and $t = 80\,\omega_p^{-1}$. In the last two thousands iterations, very thin structures are then developed. Because of its very fine resolution, the Vlasov codes are capable of resolving the finest details of particle trapping. As an example, Fig. 5 and Fig. 6 show the modulation of the distribution function followed by particle trapping in the longitudinal field and then the formation of coherent phase-space structures.

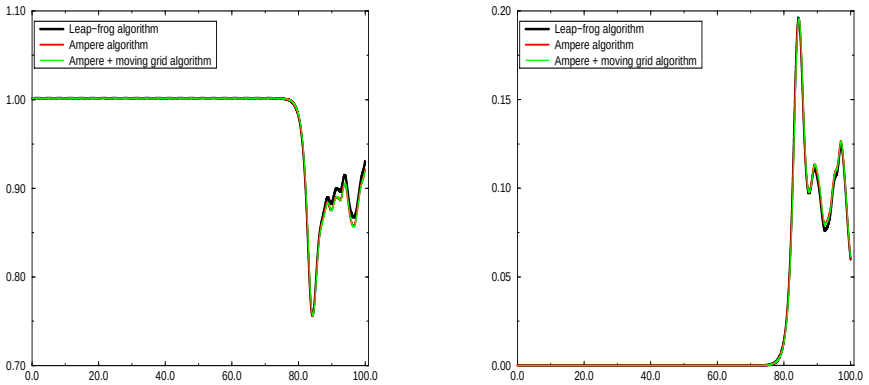

Figure 2: *Time evolution of the kinetic energy and the electric energy.*

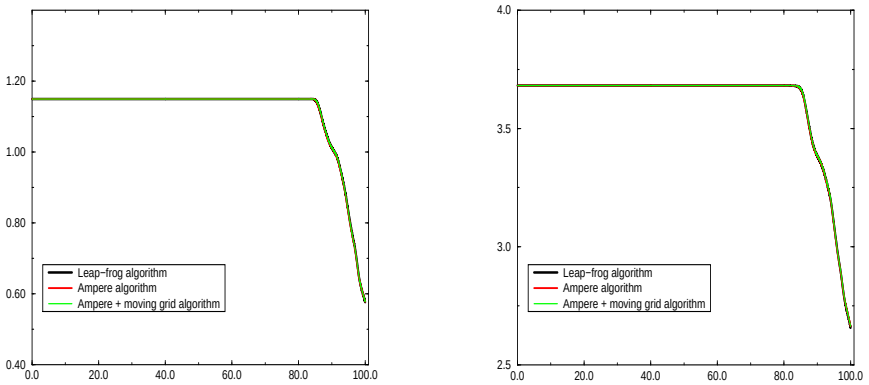

Figure 3: *Time evolution of the entropy and the L^2 norm.*

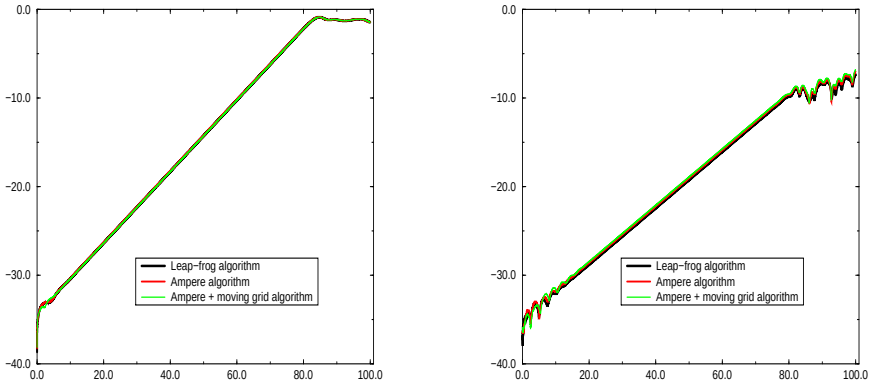

Figure 4: *Time evolution of the second mode of E_x and E_y.*

Leap-frog	15h15mn
Ampère	8h20mn
Ampère+moving grid	2h25mn

Table 1: *Time simulation for the three cases.*

However, we observe that during the major part of the simulation (between $t = 0\,\omega_p^{-1}$ and $t = 80\,\omega_p^{-1}$), many of the grid points are wasted.

Fig. 7 and Fig. 8 show the evolution of the distribution and of the phase space domain using the dynamic moving grid (and the Ampère algorithm). Beginning with a thin domain $[-0.5, 0.5]$, the domain increases according to the evolution of the instability and ends with the size $[-2.51, 2.51]$. Hence, the dynamic grid contains the whole information without needing too many points with vanishing values of the distribution function. This kind of procedure seems to overcome the major drawback of Vlasov method which is that in inhomogeneous systems, many of the grid points are wasted.

With the Ampère algorithm, the computational time is divided by 2, and the moving grid allows to obtain the same result in only 145 minutes which is more than 6 times faster than the original code (see Tab.1).

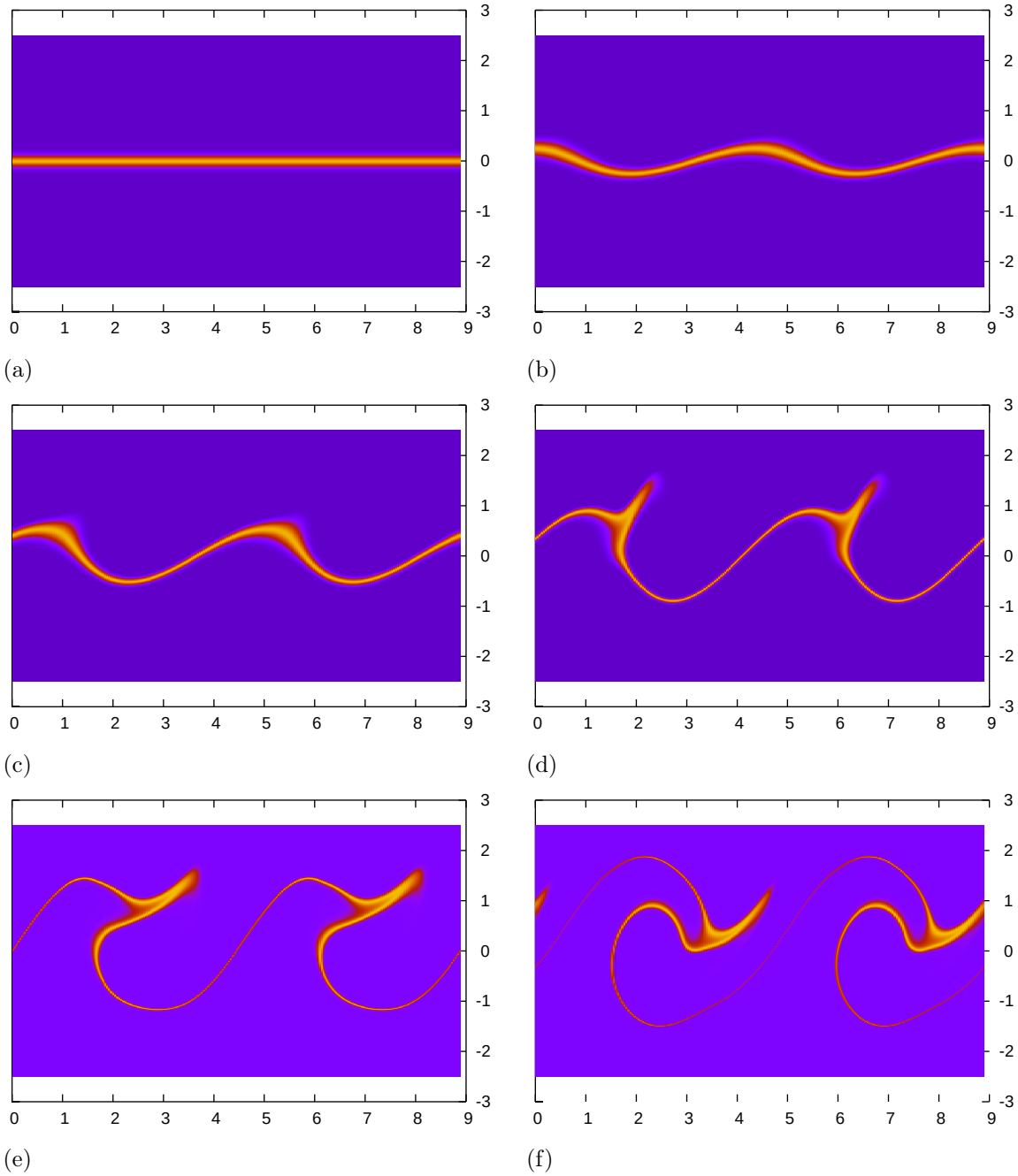

Figure 5: *Evolution of the distribution function f in the phase space.* (a) $t = 0\,\omega_p^{-1}$, (b) $t = 80\,\omega_p^{-1}$, (c) $t = 82\,\omega_p^{-1}$, (d) $t = 84\,\omega_p^{-1}$, (e) $t = 86\,\omega_p^{-1}$, (f) $t = 88\,\omega_p^{-1}$.

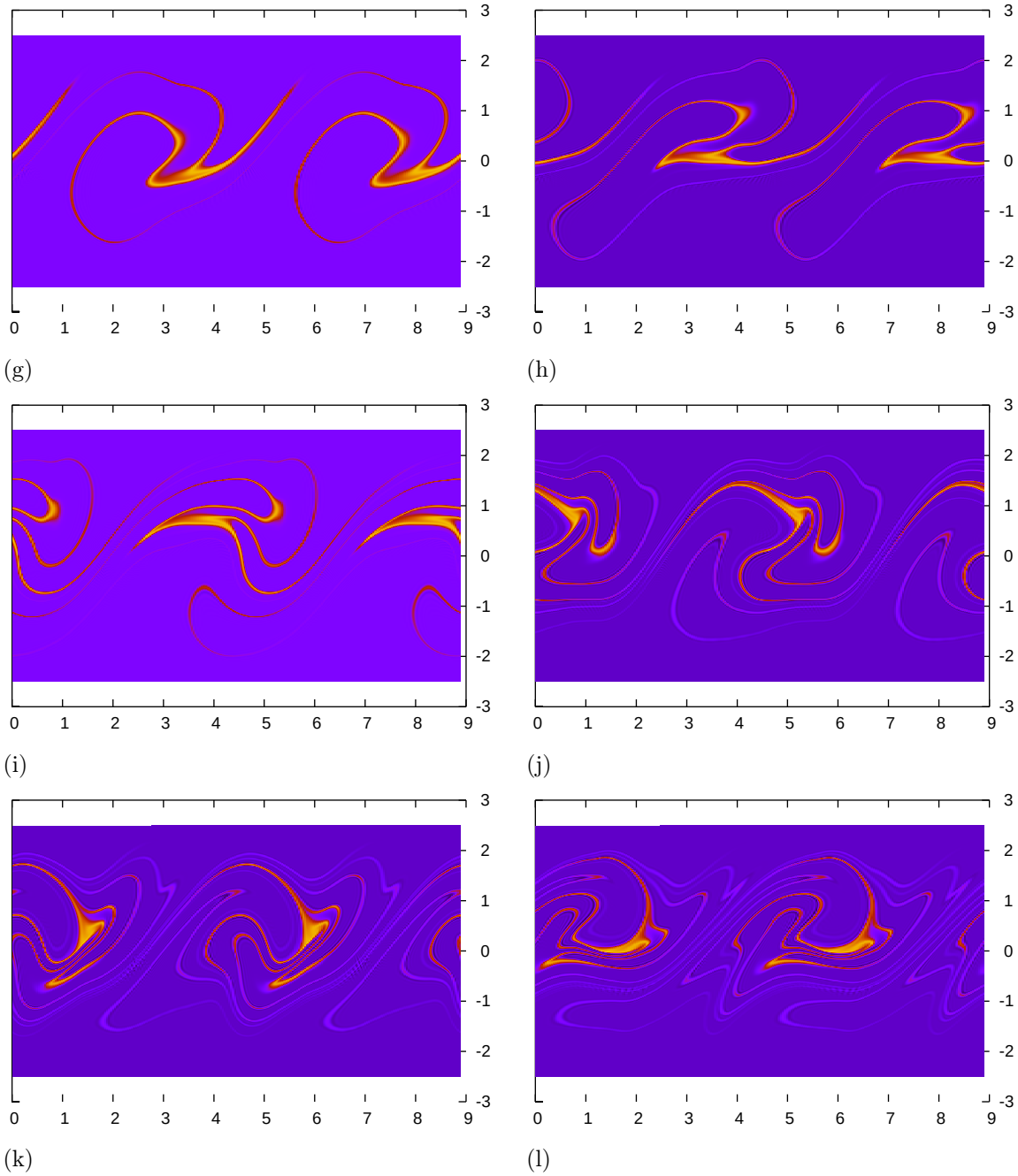

Figure 6: *Evolution of the distribution function f in the phase space.* (g) $t = 90\,\omega_p^{-1}$, (h) $t = 92\,\omega_p^{-1}$, (i) $t = 94\,\omega_p^{-1}$, (j) $t = 96\,\omega_p^{-1}$, (k) $t = 98\,\omega_p^{-1}$, (l) $t = 100\,\omega_p^{-1}$.

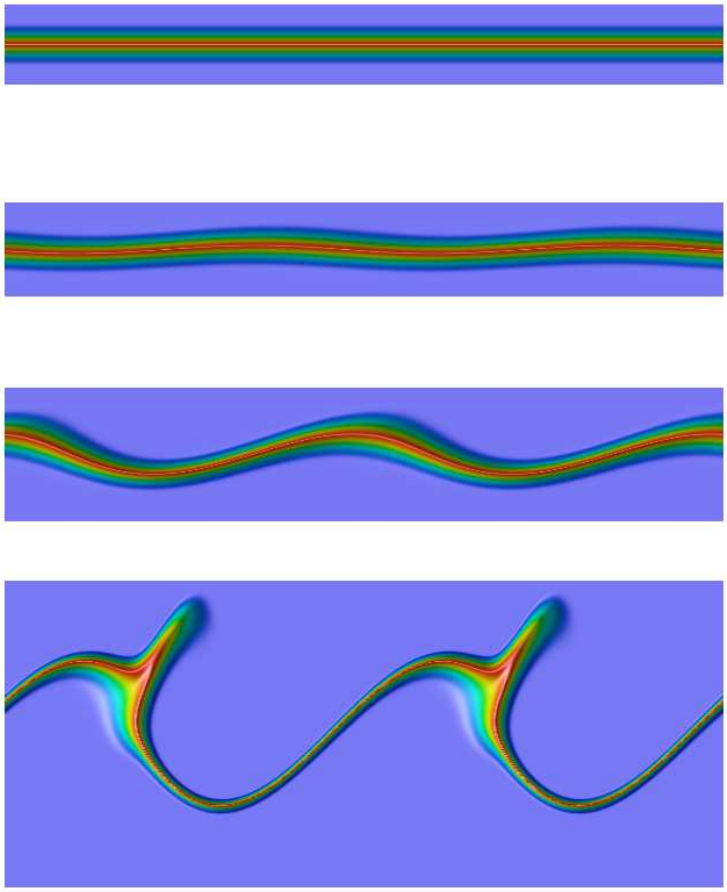

Figure 7: *Evolution of the distribution function f and of the phase space domain $[-p_{\max}, p_{\max}]$ computed with the Ampère algorithm using the dynamic moving grid.* (a) $t = 0\,\omega_p^{-1}\,p_{\max} = 0.5, (b)$ $t = 76\,\omega_p^{-1}\,p_{\max} = 0.578$, (c) $t = 80\,\omega_p^{-1}\,p_{\max} = 0.824$, (d) $t = 84\,\omega_p^{-1}\,p_{\max} = 1.902$.

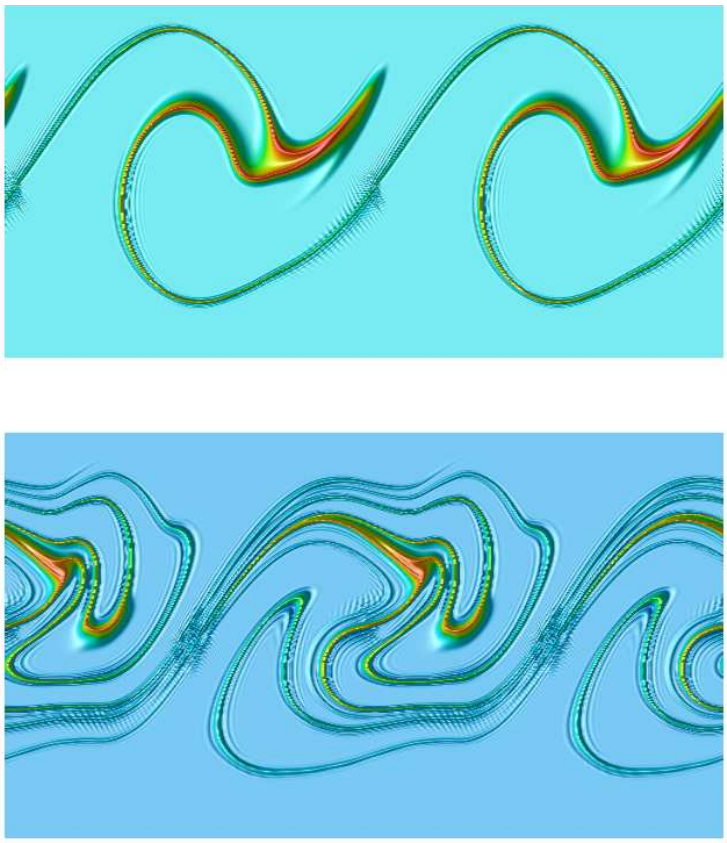

Figure 8: *Evolution of the distribution function f and of the phase space domain $[-p_{\max}, p_{\max}]$ computed with the Ampère algorithm using the dynamic moving grid.* (e) $t = 88\,\omega_p^{-1}\,p_{\max} = 2.188$, (f) $t = 96\,\omega_p^{-1}\,p_{\max} = 2.513$.

6 Conclusion

In this report, we proposed a method which appears to be very promising for relativistic applications arising in laser-plasma interaction. Starting with a Vlasov code that is able to capture thin structures using a very fine grid, we introduced an adaptive box whose size evolves according to the development of the instability. In particular, using a very simple test to increase p_{max} allows us to decrease significantly the computational cost of the initial simulations without damaging the numerical results. The reason comes from the fact that the number of grid points necessary for the simulation are considerably reduced. An extension of this work can also consider relativistic cases with open boundary conditions where the moving grid moves along the x-axis. Moreover, a future work would be envioned to beam focusing problems in which a moving grid in the phase space can follow closely the global motion of the beam.

References

[1] N. Besse, A. Ghizzo, G. Latu, E. Sonnendrücker, *A wavelet-MRA-based adaptive semi-Lagrangian method for the relativistic Vlasov-Maxwell system*, preprint, 2006.

[2] C.K. Birdsall, A.B. Langdon, *Plasma Physics via Computer Simulation*, Institute of Physics Publishing, Bristol and Philadelphia, 1991.

[3] M. Campos-Pinto, M. Merhenberger, *Adaptive numerical resolution of the Vlasov equation*, Numerical Methods for Hyperbolic and Kinetic Equation, (2004).

[4] C.Z. Cheng, G. Knorr, *The integration of the Vlasov equation in configuration space*, J. Comput. Phys., **22**, p. 330, (1976).

[5] F. Filbet, E. Sonnendrücker, *Comparison of Eulerian Vlasov solvers*, Comput. Phys. Comm., **151**, pp. 247-266, (2003).

[6] A. Ghizzo, P. Bertrand, M.L. Begue, T.W. Johnston, M. Shoucri, *A Hilbert-Vlasov code for the study of high-frequency plasma beatwave accelerator*, IEEE Trans. on Plasma Sc., **24**, p. 370, (1996).

[7] A. Ghizzo, P. Bertrand, M. Shoucri, T.W. Johnston, E. Filjakow, M. R. Feix, *A Vlasov code for the numerical simulation of stimulated Raman scattering*, J. Comput. Phys., **90**, pp. 431-457, (1990).

[8] M. Gutnic, M. Haefele, I. Paun, E. Sonnendrücker, *Vlasov simulation on an adaptive phase space grid*, Comput. Phys. Comm., **164**, pp. 214-219, (2004).

[9] F. Huot, A. Ghizzo, P. Bertrand, E. Sonnendrücker, O. Coulaud, *Instability of the time splitting scheme for the one-dimensional and relativistic Vlasov-Maxwell system*, J. Comput. Phys., **185**, pp. 512-531, (2003).

[10] F. Huot, A. Ghizzo, P. Bertrand, E. Sonnendrücker, O. Coulaud, *Study of propagation of ultraintense electromagnetic wave through plasma using semi-Lagrangian Vlasov codes*, IEEE Trans. on Plasma Sc., **28**, (2000).

[11] T.W. Johnston, P. Bertrand, A. Ghizzo, M. Shoucri, E. Filjakow, M. R. Feix, *Stimulated Raman scattering: Action evolution and particle trapping via Euler-Vlasov fluid simulation*, Phys. Fluids, **B4**, pp. 2523-2537, (1992).

[12] S. Labrunie, J.A. Carillo, *Global solutions for the one-dimensional relativistic Vlasov-Maxwell system for laser-plasma interaction*, Math. Models Methods Appl. Sci., **16**, pp. 19-57, (2005).

[13] E. Sonnendrücker, F. Filbet, A. Friedman, E. Oudet, J.L. Vay, *Vlasov simulation of beams on a moving phase space grid*, Comput. Phys. Comm., **164**, pp. 390-395, (2004).

[14] E. Sonnendrücker, J. Roche, P. Bertrand, A. Ghizzo, *The semi-Lagrangian method for the numerical resolution of the Vlasov equations*, J. Comput. Phys., **149**, pp. 201-220, (1999).

Contents

1 Introduction **3**

2 The Vlasov equation **5**

3 The semi-Lagrangian method for the Vlasov equation **6**
3.1 The semi-Lagrangian method 6
3.2 Why does the splitting fail ? 7
3.3 Algorithms for the 1D Vlasov-Maxwell system 8

4 The moving grid algorithm **11**

5 Numerical results **13**
5.1 Physical and numerical parameters 13
5.2 Results 14

6 Conclusion **21**

Unité de recherche INRIA Lorraine
LORIA, Technopôle de Nancy-Brabois - Campus scientifique
615, rue du Jardin Botanique - BP 101 - 54602 Villers-lès-Nancy Cedex (France)

Unité de recherche INRIA Futurs : Parc Club Orsay Université - ZAC des Vignes
4, rue Jacques Monod - 91893 ORSAY Cedex (France)
Unité de recherche INRIA Rennes : IRISA, Campus universitaire de Beaulieu - 35042 Rennes Cedex (France)
Unité de recherche INRIA Rhône-Alpes : 655, avenue de l'Europe - 38334 Montbonnot Saint-Ismier (France)
Unité de recherche INRIA Rocquencourt : Domaine de Voluceau - Rocquencourt - BP 105 - 78153 Le Chesnay Cedex (France)
Unité de recherche INRIA Sophia Antipolis : 2004, route des Lucioles - BP 93 - 06902 Sophia Antipolis Cedex (France)

Éditeur
INRIA - Domaine de Voluceau - Rocquencourt, BP 105 - 78153 Le Chesnay Cedex (France)
http://www.inria.fr
ISSN 0249-6399